Performance-based Seismic Assessments of Steel Fibre Reinforced Concrete Columns

Daguang Han
Southeast University
Chunli Ying
c.ying@lboro.ac.uk

Loughborough University, Leicestershire
Liyuan Chen
State Grid Pingyang Power Supply Company
Xuguang Wu
State Grid Pingyang Power Supply Company
Huizhong Lin
Wenzhou Electric Power Design Company. Ltd

Article

Keywords: steel fibre reinforced column, performance based seismic assessment, nonlinear static procedure, plastic rotation, fragility analysis

Posted Date: September 13th, 2024

DOI: https://doi.org/10.21203/rs.3.rs-4855630/v1

Additional Declarations: No competing interests reported.

Performance-based Seismic Assessments of Steel Fibre Reinforced Concrete Columns

Daguang Han[1,2]; Chunli Ying[3]*; Liyuan Chen[4];Xuguang Wu[4]; Huizhong Lin[5]

Abstract: This study presents a comprehensive investigation into the seismic performance of steel fibre reinforced concrete (SFRC) columns, aiming to assess their ductility and energy dissipation capacity. A large-scale database consisting of 116 individual tests of flexure-dominated SFRC and plain concrete (PC) columns subjected to cyclic lateral loading is utilized. The research begins by conducting parametric sensitivity analyses and empirical calibration of hysteretic parameters, crucial for accurately modelling the seismic response of reinforced concrete columns. These analyses are performed in accordance with a nonlinear static procedure. Additionally, fragility analyses of both reinforced PC and SFRC columns are conducted, based on their respective lateral drift ratios, with a specific drift ratio defined as the damage limit state. The findings of this work reveal intriguing insights. It is found that the axial load ratio has a comparable effect on the plastic rotations at the yield and ultimate points of PC and SFRC columns. However, it exhibits an entirely opposite effect on the

---

[1]Associate Professor, School of Civil Engineering, Southeast University, Nanjing, 211189, P. R. China. Email: daguanghan@seu.edu.cn.

[2] Associate Professor, Intelligent Hub for Future Engineering, Chongqing, 400000, P. R. China. Email: daguanghan@seu.edu.cn

[3] PhD, School of Architecture, Building and Civil Engineering, Loughborough University (Corresponding author).Leicestershire, LE11 3TU, UK. Email: c.ying@lboro.ac.uk.

[4] Deputy Chief Engineer, State Grid Pingyang Power Supply Company, Zhejiang Province, 325401 P.R. China. Email: lycper2002@sina.com

[4] Deputy General Manager, State Grid Pingyang Power Supply Company, Zhejiang Province, 325401 P.R. China. Email: xuguang0401@163.com.

[5] Engineer,Wenzhou Electric Power Design Company. Ltd, Zhejiang Province, 325000 P.R. China. Email: wzlhz@126.com.

rotation corresponding to the peak lateral load, especially for those with over 0.75% of fibres by volume. This discrepancy suggests that the current seismic design standards for PC columns are not directly applicable to SFRC columns. Furthermore, it is observed that the benefits of steel fibres in SFRC columns diminish at high lateral drift ratios or when flexural cracks are larger. Under these conditions, the effectiveness of fibres reduces, resulting in similar failure probabilities for both PC and SFRC columns.

Keywords: steel fibre reinforced column; performance based seismic assessment; nonlinear static procedure; plastic rotation; fragility analysis.

1. Introduction

Seismic hazards, including earthquakes, have the potential to cause significant damage to reinforced concrete structures, leading to the loss of life and economic damage to improve the seismic resistance of structures, there has been a growing interest in the use of steel fibre reinforced concrete (SFRC), a promising construction material with enhanced mechanical and durability properties and resistance to cracking at the material level. In light of the superior material properties of SFRC over that of conventional concrete, structural members manufactured using SFRC exhibit an improved resilience to withstand seismic loads, hence there are numerous applications of SFRC in civil engineering, such as elements of bridges [1-3], buildings [4-6], and industrial facilities [7-9]. Columns play a critical role in seismic-resistant design of buildings as they are responsible for resisting lateral forces during earthquakes. Building codes and standards in most countries require structures to be designed to withstand seismic forces. Thus, seismic design and assessment of reinforced concrete (RC) columns are essential for compliance with these codes and standards. This ensures the safety of occupants, maintains the structural integrity of the building, and adheres to building codes and standards. Revisiting the existing design standards for RC structures indicates that a good number of them related to the seismic evaluation of reinforced PC columns, such as ASCE41-17 [10], ACI-318-19 [11], FEMA 356 [12], International Building Code (IBC) [13], fib Model Code for Concrete Structures [14], and Eurocode 8 [15], where they provide general guidelines for the seismic evaluation of reinforced PC columns and some of them offer minimum requirements for the evaluation of existing columns to ensure adequate seismic performance. However, there is currently a lack of standardized procedures and guidelines for the seismic assessment of SFRC columns. As such, developing guidelines for the evaluation of SFRC columns is expected to be an important step towards ensuring the safe and resilient design of such structures.

Performance-based seismic assessment of RC structures has become increasingly popular in recent years as it allows for a more comprehensive and tailored evaluation of a structure's seismic performance. In such assessments, nonlinear static procedures (NSP) are commonly employed, utilizing a simplified lumped hinge model where inelastic deformation is assumed to occur solely at the hinge location, rather than being distributed along the column height (see Fig. 1(a)) [16-18]. This model helps determine the plastic hinge rotation capacity of the column (see Fig. 1(b)), representing the amount of rotation the column can experience while remaining within the elastic range of deformation. The plastic rotation capacity plays a crucial role in developing nonlinear response curves for the seismic evaluation of existing columns, as stipulated by certain standards. For example, the ASCE 41-17 standard provides a generalized force-deformation/rotation relationship for flexure-dominated RC columns, as illustrated in Fig. 1(c). This curve is utilized to evaluate the seismic performance of the column and guide any necessary rehabilitation or retrofitting measures. Fig. 2 (a) [19] shows the monotonic envelope (response curve) and cyclic response (a backbone curve) of a RC column subjected to seismic load, where for a ductile RC column that undergoes a flexure failure, four critical points in the response envelope can be used to characterize its cyclic response, including yielding-, peak-, ultimate- and collapse- points [16, 20]. Note that reaching complete collapse in laboratory tests is practically difficult due to safety considerations. Therefore, a three-point response envelope is generally considered for performance-based seismic assessments of the structures with a representative example presented in Fig. 2 (b) [21]. NSP is a useful technique in performance-based seismic design of structures and assessment because it provides a simplified representation of the structure's behaviour that can be used to evaluate its response without having to perform a detailed nonlinear analysis of the entire structure. In addition to NSP, fragility analysis is another curial tool for measuring the seismic performance of RC columns as it analyses the probability of exceeding certain limit states or performance levels under seismic loading, and is often used to evaluate the seismic risk of existing structures or to inform the design of new structures. In fragility analysis, the probability of damage or failure is typically modelled using statistical methods based on historical earthquake data, physical testing, or other sources of data [22-24]. This approach can provide a more comprehensive understanding of the potential consequences of earthquakes on structures, and can inform decision-making related to seismic design, retrofitting, and risk management.

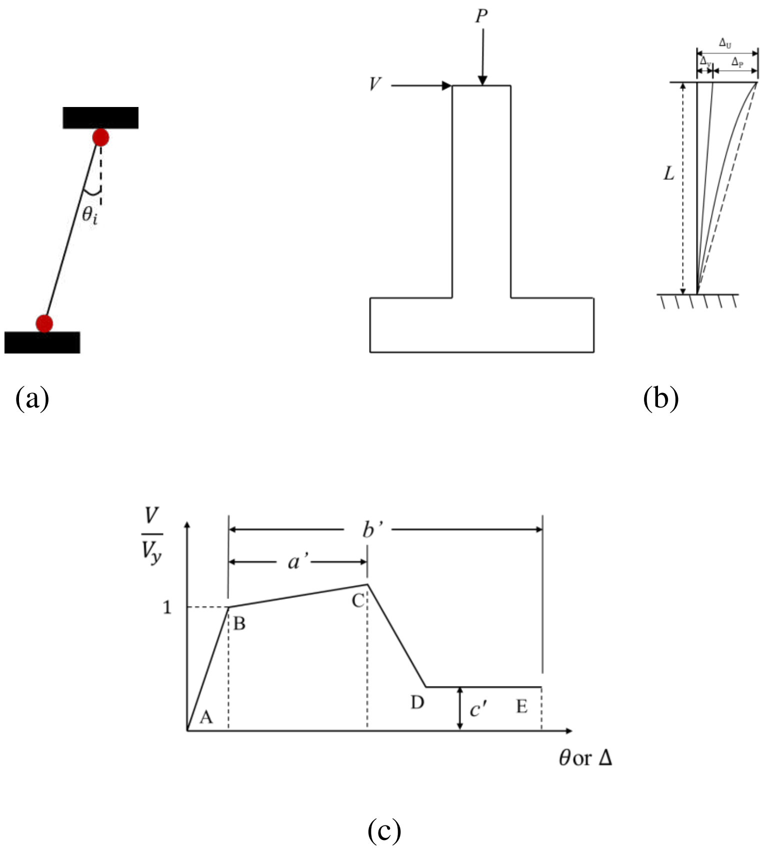

Figure 1. a) Load, displacement and chord rotation of a laterally loaded RC column; b) Moment-Rotation Plastic Hinge Model for Columns; c) Generalized force–deformation/rotation relationship for a flexure-dominated RC column in ASCE 41-17.

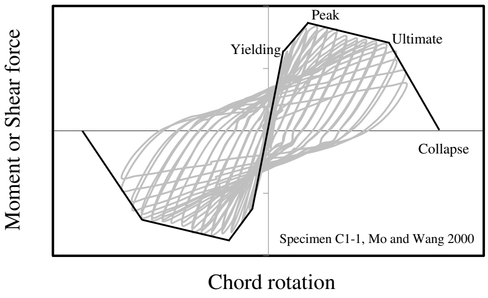

(a)

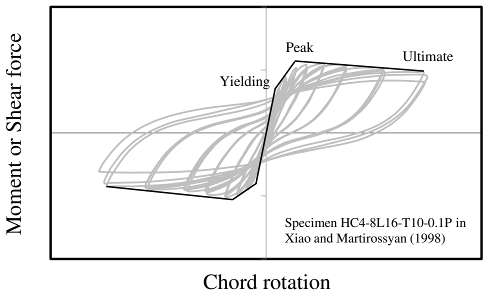

(b)

Figure 2. Monotonic envelope and cyclic response of ductile RC column subjected to combination of axial and lateral actions.

This work presents a comprehensive study to assess the seismic performance of SFRC columns, with the objective of distinguishing the design considerations between SFRC and PC columns under earthquake loading. The study begins by modelling plastic rotations on the nonlinear response curve, utilizing an experimental database comprising 116 individual tests of SFRC and PC columns subjected to cyclic lateral loading. The effects of key parameters such as axial load ratio, shear force ratio, and volumetric ratio of transverse reinforcement are quantified within these models. Drift ratios, identified on the nonlinear response curve, are employed as a proxy for damage, representing the amount of deformation or displacement experienced by a column during a seismic event. By defining a specific drift ratio as the damage limit state, fragility analysis is conducted to estimate the probability of exceeding this limit state under various seismic hazard levels. Importantly, the performance-based seismic assessment of SFRC columns in this study provides crucial insights into their behaviour and response under seismic loads. These findings contribute to the development of more effective seismic design and retrofit strategies specifically tailored for SFRC columns. Furthermore, they aid in improving guidelines and standards, particularly as a complement to ASCE 41 standard, for the utilization of SFRC columns in seismic-resistant structures.

2. Criteria for data source selection and experimental database

When compiling an experimental database on the seismic behaviour of reinforced plain concrete (PC) and steel fibre reinforced concrete (SFRC) columns subjected to lateral cyclic loading, specific selection criteria were applied and are listed as follows.:

1. Only columns constructed with steel fibre reinforced concrete are considered, whereas the test results of non-metallic fibre-reinforced concrete columns are not included; and
2. Columns should fail in bending, rather than undergoing flexure-shear or shear failure.; and
3. The information relating to load-displacement/rotation relationship of a column, either in form of a hysteretic loop or the corresponding envelope, should be illustrated; and
4. The applied lateral cyclic loading should be only monotonic, while columns tested under biaxial lateral loading condition are excluded; and
5. The geometry of, and both the longitudinal and transverse reinforcement arrangements for, each testing specimen must be provided in detail; and
6. The ancillary materials properties including fibre's characteristics and dosage, yield stress of rebars and compressive strength of concrete must be given; and
7. Due to the availability of the test data of SFRC columns with a circular cross-section (less than 10 datasets in the literature), only the experimental results of the tests of SFRC columns with a square or rectangular section and their PC columns counterparts are considered.

Based on these selection criteria, 116 datasets were compiled in the experimental database, including 80 associated with the tests of SFRC columns and 36 associated with the tests of PC columns. These test data were collected from 22 existing studies [25-45] in the literature. The parameters collated in the database are those affecting the response of RC and SRFRC under lateral cyclic loading, including the geometry of each testing specimen, longitudinal reinforcement ratio (ρ_l)), transverse reinforcement reported in both volumetric (ρ_{t_v}) and areal ratio (ρ_{t_a}), axial load ratio ($\frac{P}{A_g f_c}$), shear force ratio ($\frac{V}{bd\sqrt{f_c}}$), fibre's characteristics (fibre's length, l_f and diameter, d_f) and volume fraction (v_f). The range and distribution of each selected parameter are shown in Fig. 3. Note that the cubic compressive strength of concrete in some works was converted to the equivalent cylindrical compressive strength by the method reported in [46] to unify the measure of the compressive strength of concrete in the database. The fibre reinforcing index (*RI*) shown in Fig. 3 (g), which is commonly used to quantify the effect of discrete fibre in concrete, can be calculated as:

$$RI = v_f \frac{l_f}{d_f} \tag{1}$$

As introduced before, the seismic response of a reinforced concrete (RC) column can be characterized by an idealized hysteresis envelope, which accommodates the yielding, peak, and ultimate points of the column's response under seismic loading. However, in many cases, experimental data on the actual values of these key points on the envelope of a hysteresis curve of RC columns are not available. More than two-thirds of the test series in the current database lack information of these critical points. To overcome this limitation, the current study proposes alternative definitions of lateral drifts or chord rotations corresponding to the three critical points based on available test results and commonly used methods reported in the literature [22, 47, 48]. These alternative definitions are graphically depicted in Fig. 4, and the values acquired from them are included in the complete database as shown in Tables S1 and S2 in Supplementary Materials.

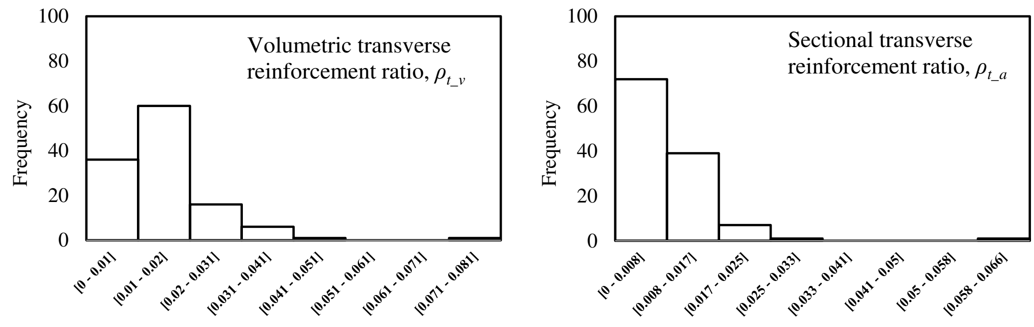

(a) (b)

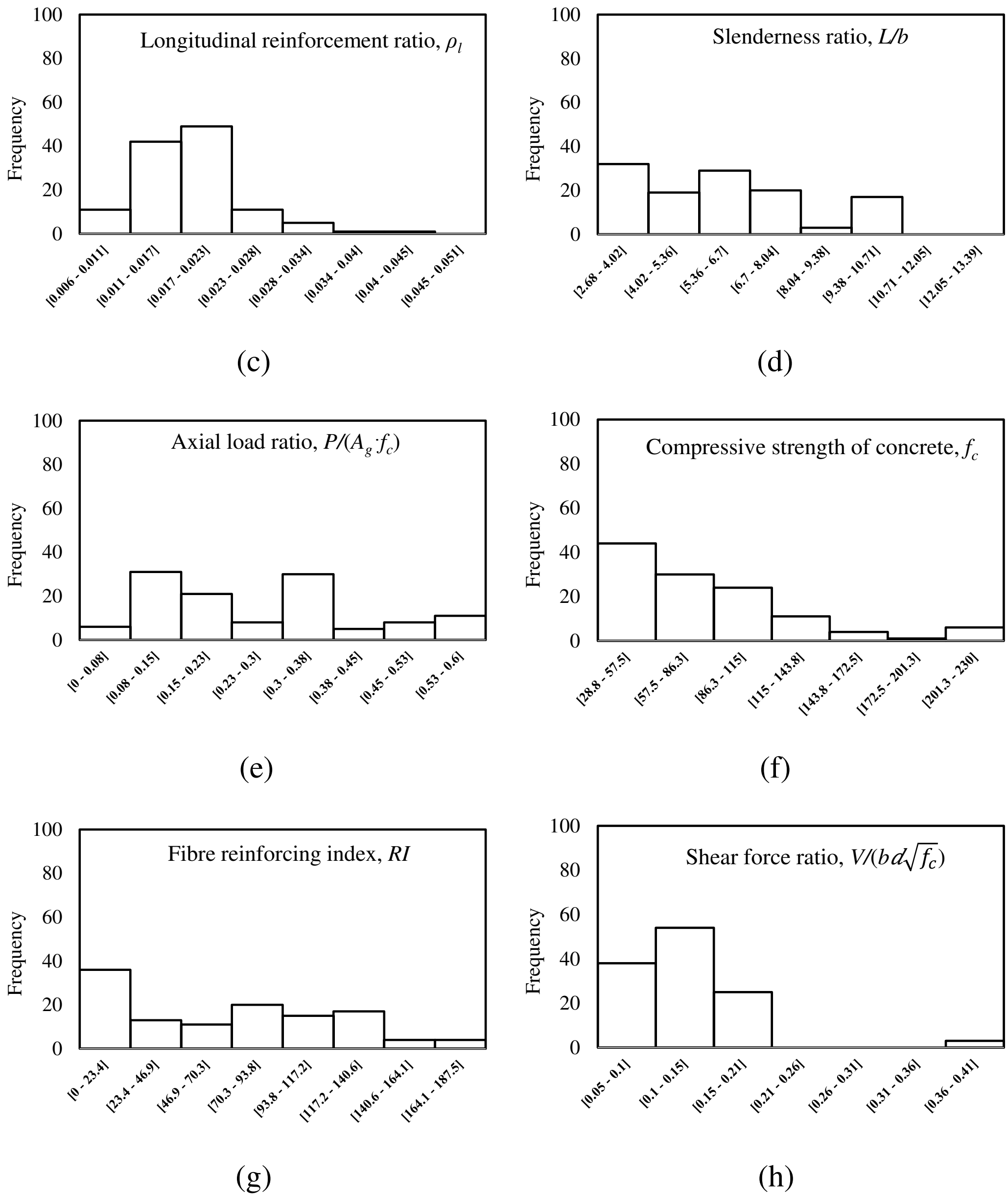

Figure 3. Distributions of the key factors.

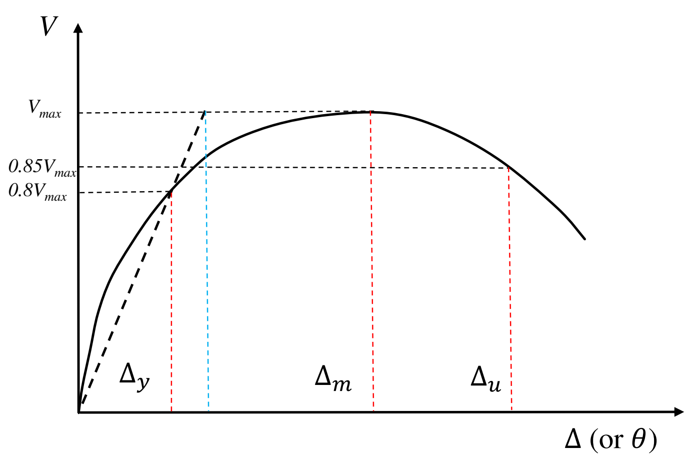

Figures 4. Definitions of alternative drift ratios.

3. Effects of key factors on lateral drift ratio of reinforced PC or SFRC columns under cyclic lateral loads

This section explores the impacts of several factors on the behaviour of PC and SFRC columns when subjected to a cyclic lateral load, including the geometry of the specimen, material properties, and applied load level. Specifically, the quantitative implications of these factors for the lateral drift ratio of reinforced PC or SFRC columns are presented and discussed.

It is well-established in the literature that the slenderness of an RC column is a significant factor that affects the column's lateral drift under seismic loading. As the slenderness ratio increases, the column tends to deflect more laterally [49-51]. By examining the results in the global database, Fig. 5 illustrates the correlations between depth-to-shear span ratio (*b/L*) and lateral drift ratio (θ_i) of either PC or SFRC column at different lateral deflection levels. It is evident that *b/L* is a decisive factor influencing the lateral drift ratios (θ_i) measured at the yielding, peak and ultimate points. The relationship between the $\theta_i/(b/L)$ and b/L can be represented by an exponential function with a generic form of:

$$\theta_i/(b/L) = x_{1-i} exp^{-X_{2-i}\cdot(b/L)} \quad (2)$$

where x_{1-i} and x_{2-i} are empirical coefficients in the models for the lateral drift ratio θ_i at each of the three points ($i = y, m, u$), with their specific values summarised in Table. 1. It should be noted that when using *b/L* as the sole parameter to predict θ_y, θ_m and θ_u, some level of data dispersion is observed. This implies that incorporating other parameters might improve the prediction accuracy. In the remainder of this section, the influences of other factors on lateral drift of PC and SFRC columns under seismic loading are evaluated.

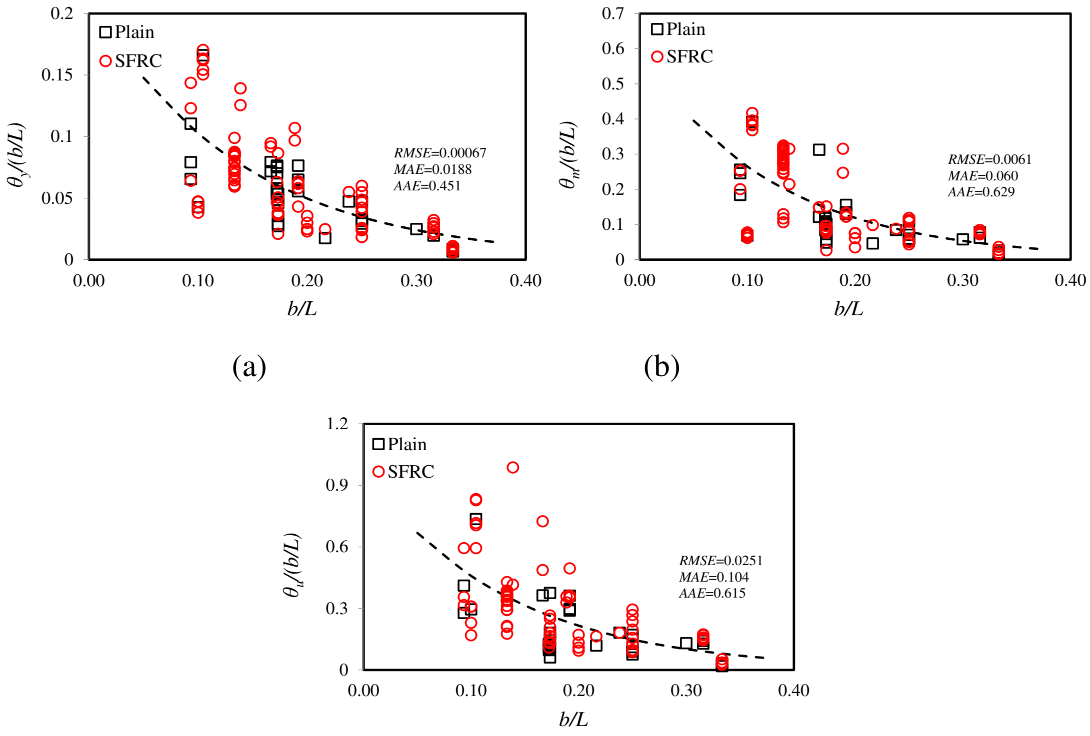

(c)

Figure. 5 Effect of a/L on the lateral drift ratio at: a) yielding; b) peak; and c) ultimate points.

Table 1. Empirical coefficients for the developed models

Drift ratio	x_{1-i}	x_{2-i}	x_{3-i}	x_{4-i}	x_{5-i}	x_{6-i}
θ_y-*Mod1*			1.26	0.23	0.22	0.20
θ_y-*Mod2*	0.21	7.27	1.37	1.16	2.60	11.72
θ_y-*Mod3*			1.21	12.67	0.74	1.62
θ_m-*Mod1* ($v_f \leq 0.75$)			0.57	0.09	0.08	0.33
θ_m-*Mod2* ($v_f \leq 0.75$)	0.59	8.01	1.44	0.96	0.97	44.80
θ_m-*Mod3* ($v_f \leq 0.75$)			1.28	11.80	0.02	3.20
θ_m-*Mod1* ($v_f > 0.75$)			1.86	0.29	-	0.36
θ_m-*Mod2* ($v_f > 0.75$)	0.59	8.01	1.30	1.18	-	22.34
θ_m-*Mod3* ($v_f > 0.75$)			1.23	15.23	-	2.63
θ_u-*Mod1*			0.89	0.14	0.22	0.17
θ_u-*Mod2*	0.97	7.53	1.49	1.06	2.59	8.32
θ_u-*Mod3*			1.30	2.74	0.67	1.45

Axial load ratio ($\frac{P}{A_g f_c}$) is an essential factor that affects the seismic behaviour of RC column. In the NSP of the ASCE 41-17 standard, $\frac{P}{A_g f_c}$ is selected as a parameter to model the plastic rotation of

RC column. Fig. 6 presents the results of several individual experimental campaigns with $\frac{P}{A_g f_c}$ is the only variable, showing the effect of axial load ratio on the lateral drift ratio at the yielding, peak, and ultimate points in the envelope for load-lateral rotation hysteresis loop of SFRC. It can be seen that for most of the cases, the lateral drift ratio decreases with an increase in $\frac{P}{A_g f_c}$. This is consistent with that is quantified in ASCE 41-17, where a negative empirical coefficient is assigned to $\frac{P}{A_g f_c}$ when predicting plastic rotation angle of an RC column. This can be explained by the fact that an increased $\frac{P}{A_g f_c}$ results in a higher level of confinement to the column axially, which, in turn, prevents its lateral deformation.

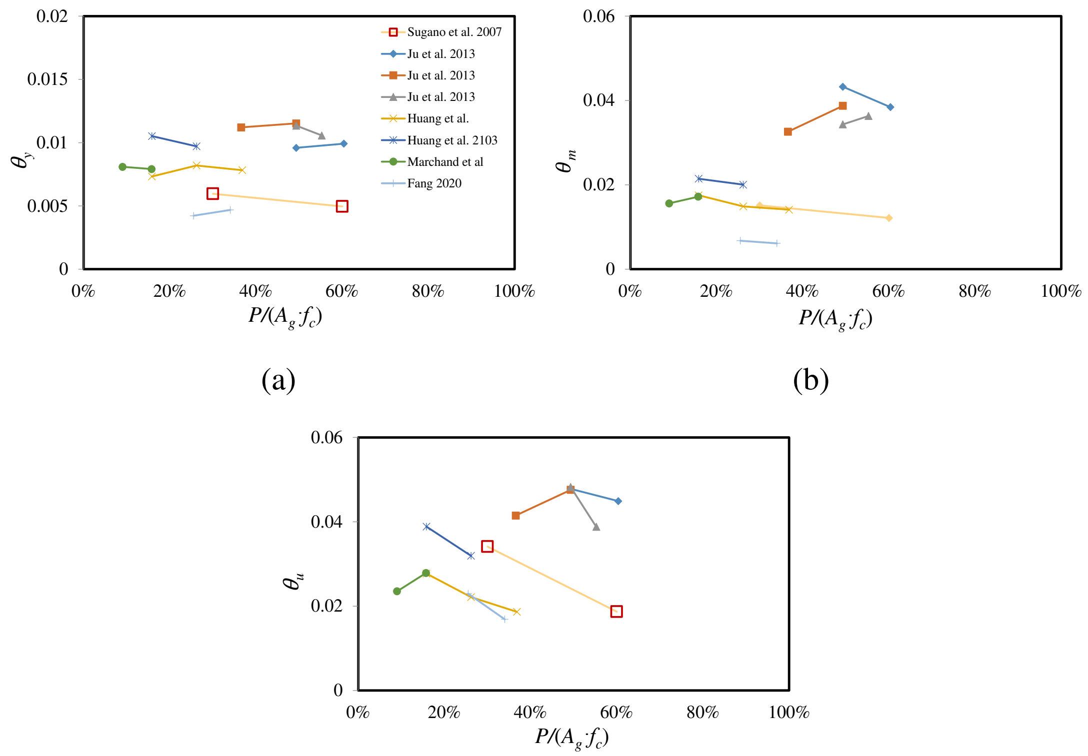

(a) (b)

(c)

Figure 6. Effect of axial load ratio on lateral drift ratio at: a) yielding; b) peak; and c) ultimate points.

However, for a SFRC column, the influence of $\frac{P}{A_g f_c}$ on its $\theta_m$is ambiguous. As shown in Fig.6, the results of a several studies shows an opposite trend where a larger $\frac{P}{A_g f_c}$ leads to a higher θ_i even at a relatively higher $\frac{P}{A_g f_c}$ level (>50%). Closer inspections of them reveals that the specimens associated with the contrary findings contain a higher volume fraction of steel fibres, 1.3% for those tested by Ju et al. [31] and 2.5% for those tested by Marchand et al. [39]. This phenomenon is attributed to the alignment of discrete fibres with the axial direction under a higher level of axial load. When the fibres are oriented more axially under a higher level of axial load, they are less effective at bridging and arresting cracks in the lateral direction, leading to a higher lateral drift ratio, where this impact is particularly significant for the specimen with a higher fibres' dosage. For those columns containing a lower fraction of fibres, the effect of $\frac{P}{A_g f_c}$ on their performances is similar to that on PC columns.

Beyond the assessments using results reported locally, e.g., from individual experiments, the evaluations of $\frac{P}{A_g f_c}$ on the seismic response of PC and SFRC columns are undertaken with the support of the global database. To do this, each θ_m is first normalized by its predicted value using Eq. (2) to eliminate the effect of *b/L* ratio. The effect of $\frac{P}{A_g f_c}$ on θ_y, θ_m and θ_u are shown in Fig. 7 (a) to (c), respectively. The global trendline for each dataset was developed based on the best-fitted model. It is evident that $\frac{P}{A_g f_c}$ possesses similar effect on θ_y and θ_u of PC and SFRC columns (see. Fig. 7 (a) and (c)). This can be attributed to: 1) at yielding, the lateral deflection of a RC column is primarily governed by its flexural stiffness and strength, which are independent of the axial load ratio; 2) at the ultimate stage, as the column has already undergone significant damage, its lateral load-carrying capacity is predominated by its strength and ductility not the applied axial load ratio. Nevertheless, the effect of $\frac{P}{A_g f_c}$ on θ_m of PC and SFRC columns is distinct. As shown in Fig. 7 (b), a higher $\frac{P}{A_g f_c}$ results in a smaller θ_m of the columns without or containing lower content of fibres (<0.75% by volume, which is explained in detail later in this paper), in agreement with those reported in the existing literature [27, 34] and ASCE 41-17 standard for RC columns. Whereas the θ_m of SFRC that contains over 0.75%

fibres increases marginally with an increase in $\frac{P}{A_g f_c}$, where the possible mechanism governing this action is explained previously. Therefore, a unified model which contains $\frac{P}{A_g f_c}$ is possibly applicable to predict the lateral drift ratio of PC and SFRC columns at the yielding or ultimate point, whilst it is necessary to differentiate the models for θ_m of PC and SFRC columns using $\frac{P}{A_g f_c}$.

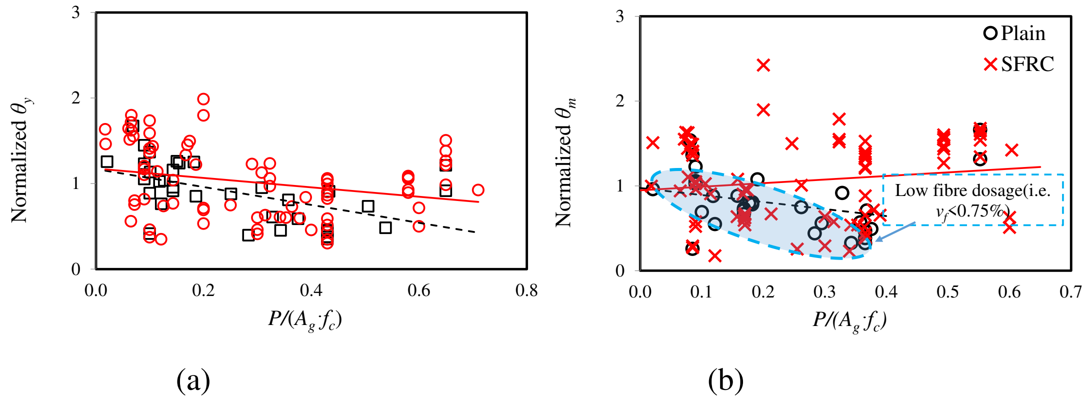

Figure 7. Effect of axial load ratio on the normalized lateral drift ratio corresponding to yielding, peak and ultimate points-analysis based on the global database.

The third parameter chosen for evaluation is shear force ratio, which is formulated as $\frac{V}{bd\sqrt{f_c}}$, where V is shear force corresponding the flexural capacity (M) of a column section and can be calculated as $V = \frac{M}{L}$; the width and depth of the column section are denoted as b and d, respectively; f_c is the cylindrical compressive strength of the concrete used to manufacture the column. Note that the flexural capacity of a reinforced PC column section can be empirically calculated using the method as per reported in ACI 318-19 as recommend in the previous studies [47, 48]. However, in this work for more accurately quantify the fibres' contribution to the flexural capacity of SFRC columns, especially at the post-cracking stage of a column under bending, the V of each column section was numerically generated using a partial-interaction mechanics-based model for FRC flexural member, in which the detailed modelling procedure can be found in the authors' previous work [52]. The correlation between the normalized θ_i and $\frac{V}{bd\sqrt{fc}}$ is illustrated in Fig. 8. It shows that, the effect of $\frac{V}{bd\sqrt{fc}}$ on θ_i of PC and SFRC column follows a similar trend, where θ_i decreases with increasing $\frac{V}{bd\sqrt{fc}}$. This is in support of those report in the previous studies on RC columns [47, 48, 53] and is aligned with the negative sign for $\frac{V}{bd\sqrt{fc}}$ in the model for plastic rotation in ASCE 41-17, which is simply attributed to the improved shear capacity of a column to resist a higher lateral load without experiencing significant deformation. Although there are minor differences between the trendlines in Fig. 8 for PC and SFRC columns, a unified model containing $\frac{V}{bd\sqrt{fc}}$ is possibly applicable to predict the lateral drift ratio of PC and SFRC columns.

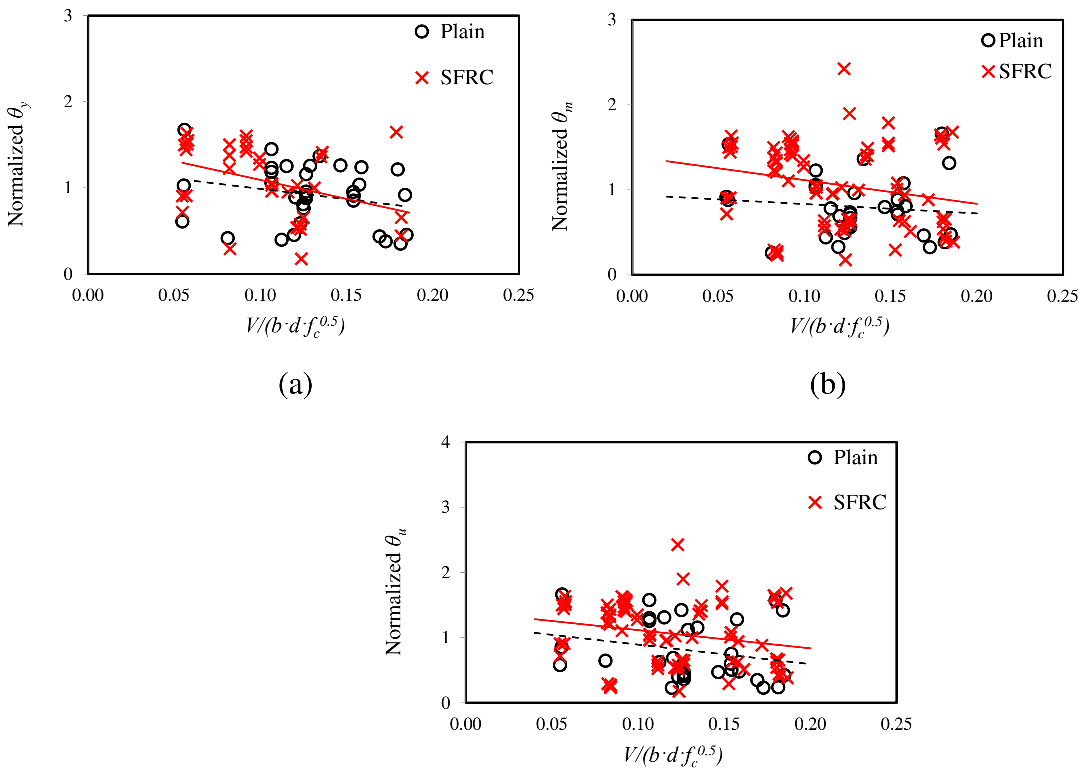

(c)

Figure 8. Effect of shear force ratio on the normalized lateral drift ratio corresponding to the peak and ultimate point-analysis based on the global database.

The final parameter considered is the transverse reinforcement volumetric ratio, and its effect on the seismic behaviour of PC and SFRC columns is assessed. The primary role of transverse reinforcement ratio in RC columns is to provide confinement to the longitudinal reinforcement and inner concrete to improve the column's ductility and shear strength. In addition, stirrups help to control the width and spacing of the cracks that occur in the column, which can affect the column's lateral drift. It is worth noting that in a SFRC column, steel fibres are additions to the conventional transverse reinforcement to offer inner confining effect and shear resistance, which enhances the columns' performance under seismic load [53]. Fig. 9 illustrates the effect of fibre volume content on θ_i using the results from individual experimental campaigns where the fibre volume fraction is the only varied factor. As expected, owing to the internal confining effect and shear resistance offered by the fibres, a higher dosage of fibres in concrete generally enhances the ductility of the corresponding column, allowing larger lateral drift ratios corresponding to yielding, peak and ultimate points. That is θ_i increases slightly with increasing fibre volume at all stages of loading. To evaluate and the quantify the overall effects of steel fibres and stirrups in the transverse direction, the confinement stress (f_{l_fib}) due to the fibres' actions is first calculated in accordance with the model suggested by [43, 54]:

$$f_{l\_fib} = \frac{3}{8} v_f \frac{l_f}{d_f} \tau_f \quad (3)$$

where v_f, l_f and d_f are fibres' volume fraction, length (in mm) and nominal diameter (in mm); τ_f is the bond stress between individual fibre and concrete matrix, where τ_f= 5.4 MPa is suggested [43, 55]; $\frac{3}{8}$ is the fibre orientation efficiency factor as specified in [43, 56]. Fibres' confining effect can be converted to equivalent transverse reinforcement ratio via:

$$\rho_{fib\_eq} = \frac{f_{l\_fib}}{f_{yt}} = \frac{\frac{3}{8} v_f \frac{l_f}{d_f} \tau_f}{f_{yt}} \tag{4}$$

where f_{yt} is the yielding stress of stirrup.

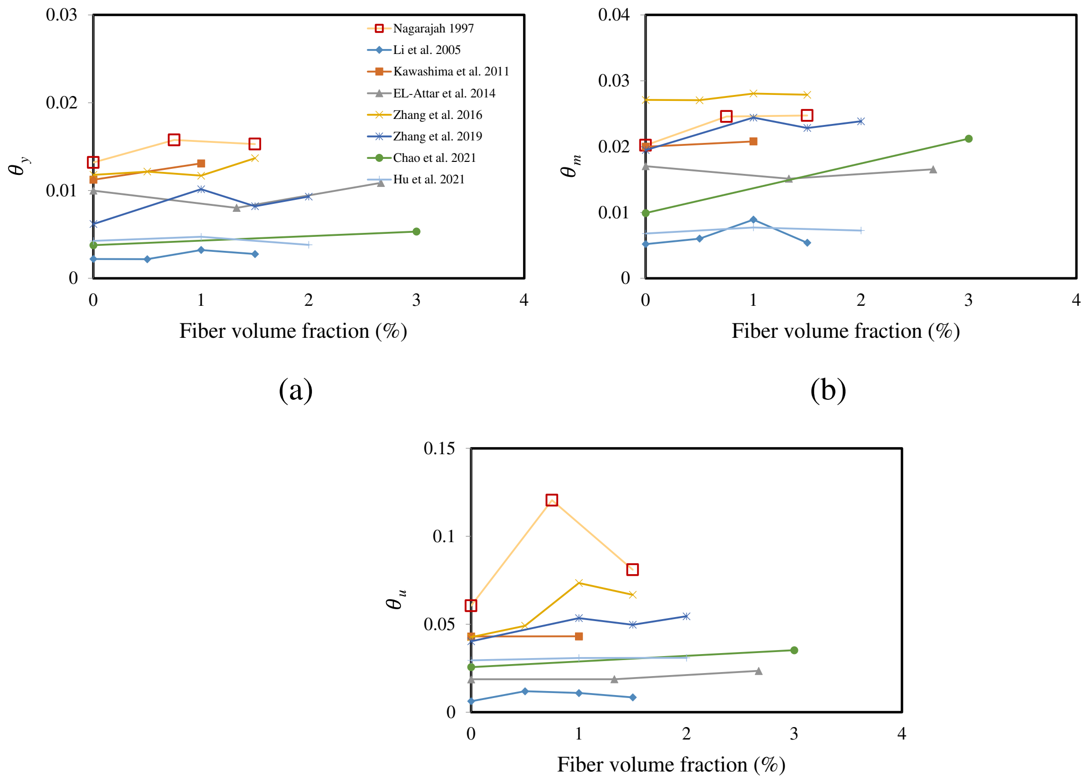

(a) (b) (c)

Figure 9. Effect of fibre volume content on lateral drift ratio at: a) yielding; b) peak; and c) ultimate points.

The overall transverse reinforcement volumetric ratio is:

$$\rho_{t\_eq} = \rho_t + \rho_{fib\_eq} \tag{5}$$

Figure. 10 shows the effect of ρ_{t_eq} on θ_x, from which it can be seen that as expected a higher ρ_{t_eq} leads to a larger θ_x at all the drift levels, which is attributed to the enhanced confinement provided by the transverse reinforcement and fibres. Moreover, the trendlines for the companion PC and SFRC columns' results show in the figure are similar, which confirm the validity of the applied method for converting fibres' contribution to the equivalent transverse reinforcement volumetric ratio and also implies that a unified model considering ρ_{t_eq} is possibly applicable to predict the lateral drift ratio of

PC and SFRC columns.

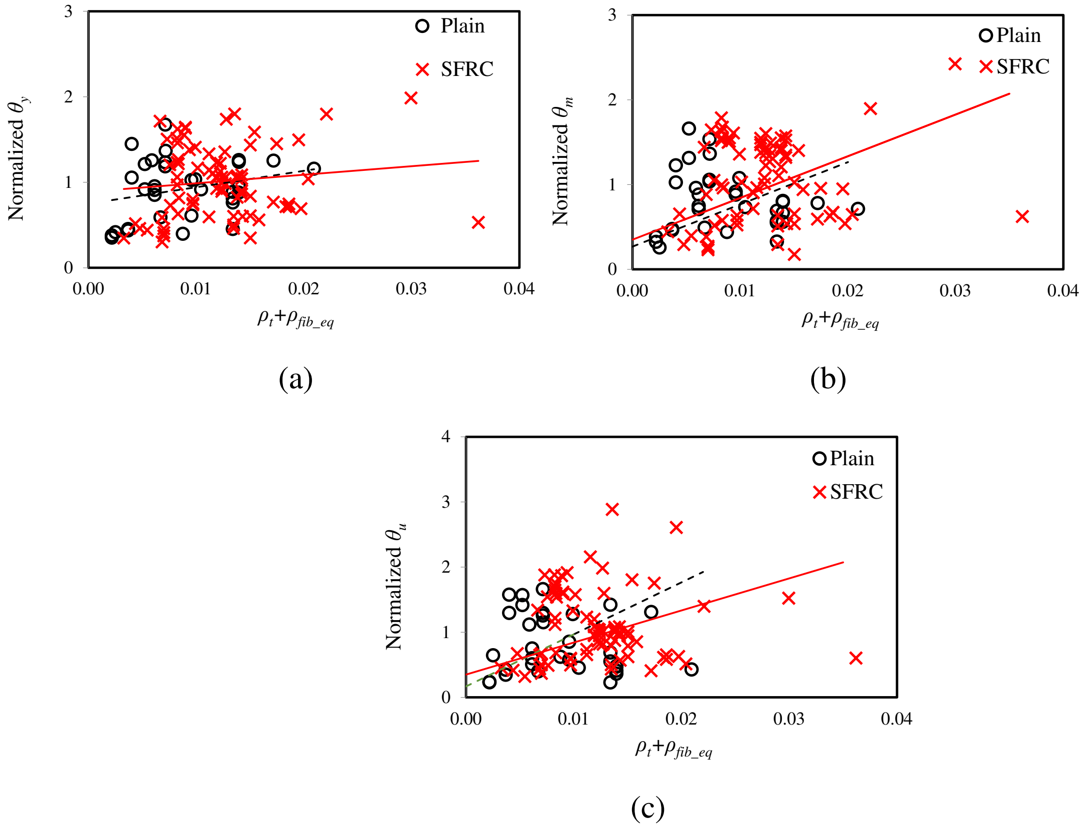

Figure 10. Effect of total equivalent transverse reinforcement ratio on the normalized lateral drift ratio corresponding to the peak and ultimate point-analysis based on the global database.

4. Modelling chord rotations for the response envelope

After assessing the effects of the identified factors on the lateral drift ratio of PC and SFRC columns under seismic load, in this section the models for chord rotations for their response envelopes are presented. The modelling parameters for θ_y, θ_m and θ_u are b/L, $\frac{P}{A_g f_c}$, $\frac{V}{bd\sqrt{f_c}}$ and ρ_{t_eq}. Three generic model expressions (Eqs. (6)-(8)) are selected and refined using those reported in [10, 16, 48] respectively. The empirical coefficients for each model were calibrated against the experimental results in the database by means of least squares method.

$$\frac{\theta_i}{b/L} = x_{1-i} \cdot e^{-x_{2-i}(b/L)} \cdot \left(x_{3-i} \cdot \left(\rho_{t\_eq}\right)^{x_{4-i}} \cdot \left(\frac{P}{A_g f_c}\right)^{-x_{5-i}} \cdot \left(\frac{V}{bd\sqrt{f_c}}\right)^{-x_{6-i}}\right) \quad (6)$$

$$\frac{\theta_i}{b/L} = x_{1-i} \cdot e^{-x_{2-i}(b/L)} \cdot \left(x_{3-i} \cdot (x_{4-i})^{100\rho_{t\_eq}} \cdot (x_{5-i})^{-\frac{P}{A_g f_c}} \cdot (x_{6-i})^{-\frac{V}{bd\sqrt{f_c}}} \right) \quad (7)$$

$$\frac{\theta_i}{b/L} = x_{1-i} \cdot e^{-x_{2-i}(b/L)} \cdot \left(x_{3-i} + 1.28 + x_{4-i} \cdot \left(\rho_{t\_eq}\right) - x_{5-i} \cdot \left(\frac{P}{A_g f_c}\right) - x_{6-i} \cdot \left(\frac{V}{bd\sqrt{f_c}}\right) \right) \quad (8)$$

Note that when modelling the θ_m using the global database, as stated previously, the effect of $\frac{P}{A_g f_c}$ is different for PC and SFRC columns. Through a serval trail-error process, v_f of 0.75% was identified as a threshold that can be applied to subset the database. As indicated in Fig. 8 (b), the effect of $\frac{P}{A_g f_c}$ on θ_m of SFRC columns containing less than 0.75% fibres and PC concrete column are nearly identical, where a higher $\frac{P}{A_g f_c}$ results in a lower θ_m. Based on the statistical analysis, the effect of $\frac{P}{A_g f_c}$ on θ_m of SFRC columns containing more than 0.75% fibres is however insignificant, hence the item associated with $\frac{P}{A_g f_c}$ in each corresponding model can be removed without affecting the model's performance. The values of the empirical coefficients x_{1-i} to x_{6-i} are summarized in Table 1 for each θ_i. In addition to that graphically presented in Figs 11 to 13, the models' performances assessed using statistical indicators including root mean square error (*RMSE*), mean square error (*MAE*), absolute average error (*AAE*), standard deviation (*SD*) and mean value are also given in Table 2. All the three developed models can adequately predict chord rotation θ_y, θ_m and θ_u, where the model form taken from [48] preforms slightly better than the other two.

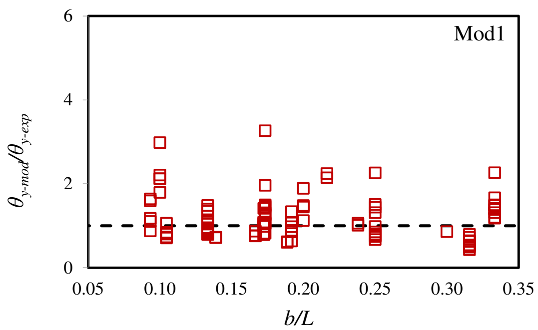

(a)

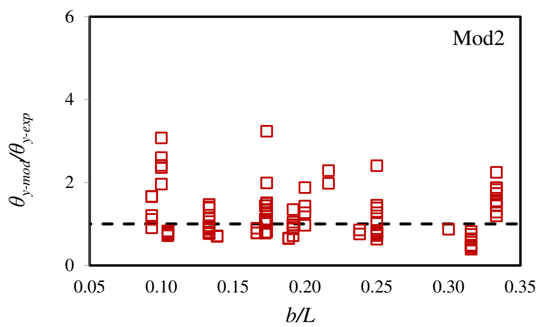

(b)

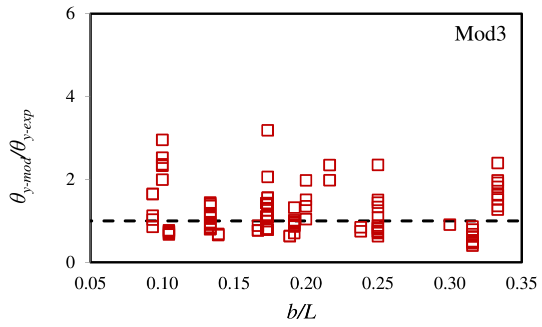

(c)

Figure 11. Performance of model for normalized rotation at the yielding point.

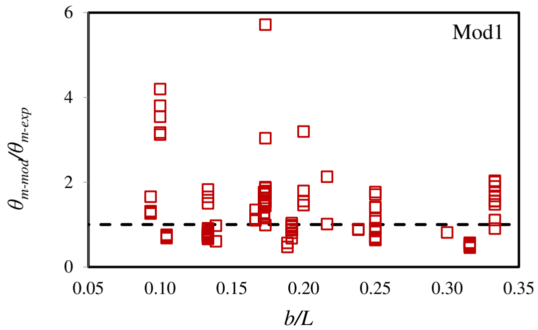

(a)

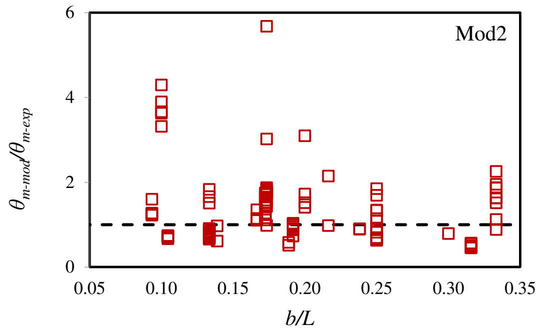

(b)

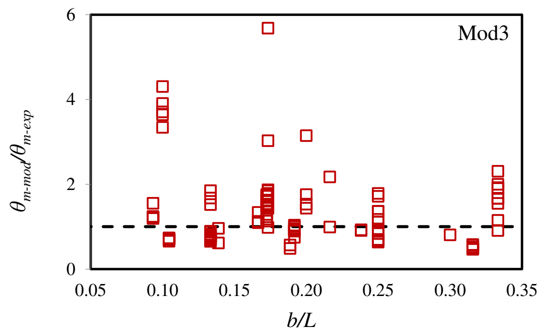

(c)

Figure 12. Performance of model for normalized rotation at the peak point.

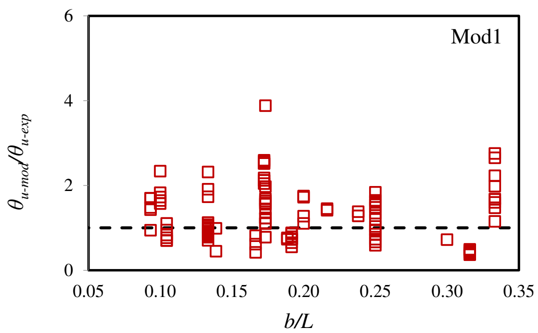

(a)

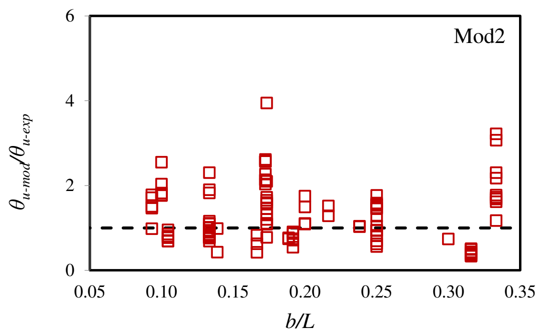

(b)

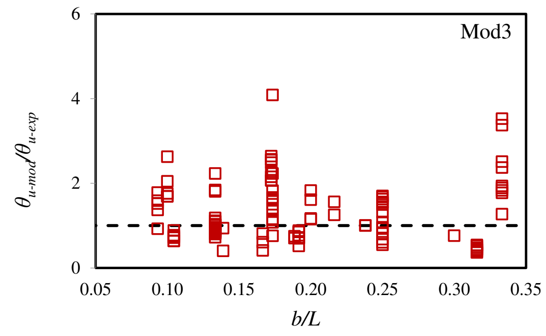

(c)

Figure 13. Performance of model for normalized rotation at the ultimate point.

Table 2. Performances of the calibrated models.

Type of model	Property	*RMSE*	*MAE*	*AAE*	Mean	*SD*
Mod1	θ_y	0.1%	1.9%	45.1%	1.24	0.62
	θ_m	21.9%	37.7%	54.9%	1.28	0.69
	θ_u	26.3%	39.5%	50.6%	1.25	0.41
Mod2	θ_y	0.1%	1.9%	45.1%	1.24	0.62
	θ_m	21.9%	37.9%	55.8%	1.29	0.73
	θ_u	27.6%	40.3%	52.8%	1.27	0.46
Mod3	θ_y	0.1%	1.9%	45.1%	1.24	0.62
	θ_m	22.3%	38.1%	56.2%	1.29	0.74
	θ_u	28.2%	41.3%	55.0%	1.29	0.50

Having established the models for θ_y, θ_m and θ_u, the plastic rotation angles a' and a'' , which are the parameters to account for the inelastic behaviour of the column beyond the yield point, are subsequently calculated. Note that the a' is defined the same way as in ASCE 41-17 (see Fig. 14), which is the difference between the rotation at peak strength and the rotation at yield strength:

$$a' = \theta_m - \theta_y \tag{9}$$

Owing to the availability of the experimental data in the literature, instead of using the rotation angle of a column at collapse, in the current paper, the maximum rotation is defined as that the column can sustain before reaching a state unacceptable damage, as defined previously in this paper (e.g., θ_u, which is the rotation angle corresponding to the point of 15% drop in strength from the peak) as presented in Fig. 14. The plastic rotation relating to the range between the yield point and the unacceptable damage state can be calculated as:

$$a'' = \theta_u - \theta_y \tag{10}$$

The values of the two plastic rotation parameters a' and a'' can be obtained by substituting the developed models for θ_y, θ_m and θ_u into Eqs. (6) and (8). The performances of the models are graphically illustrated in Figs. 15 and 16 for different model forms, where it can be seen that the predicted- and experimental- values generally correlate well.

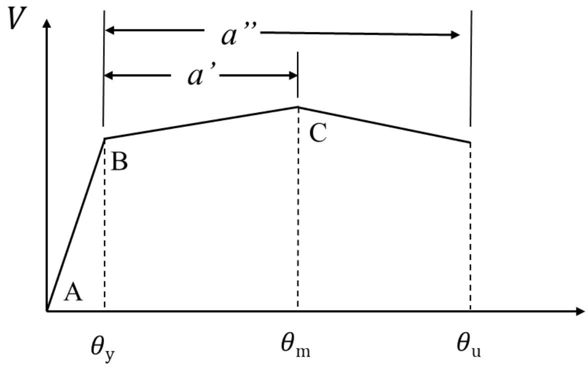

Figure 14. Definitions of plastic rotations.

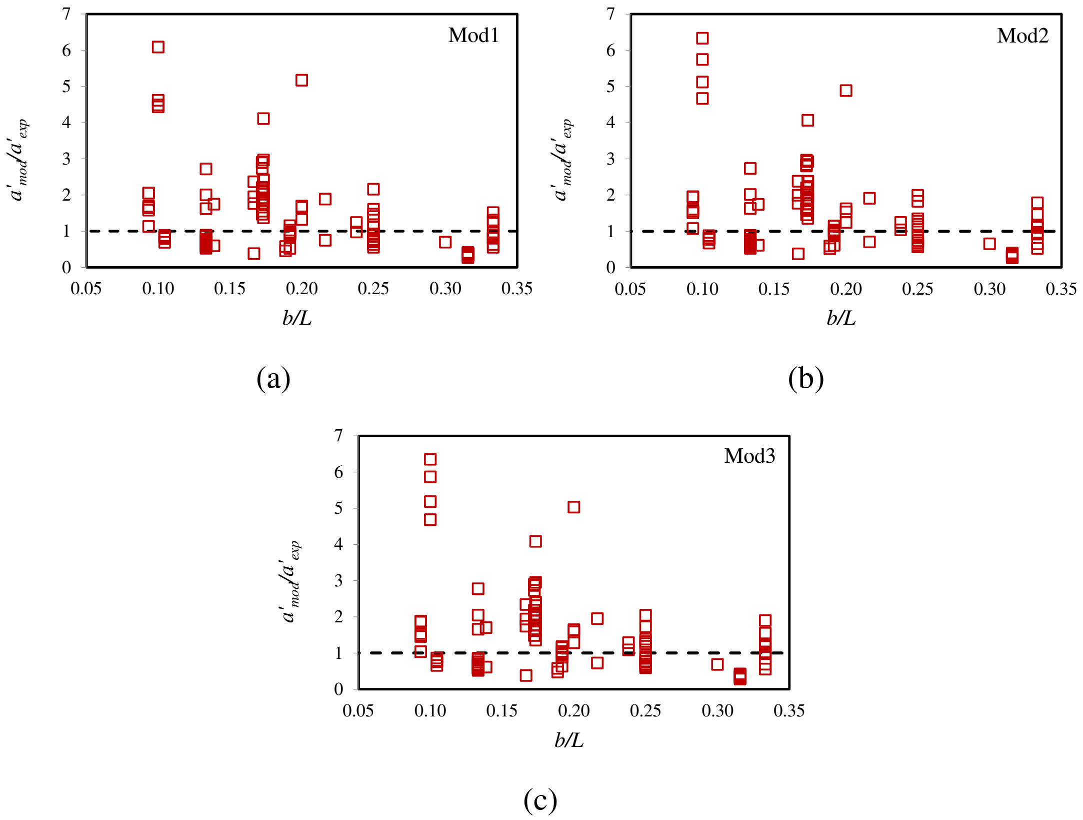

Figure 15. Performance of model for plastic rotation a'.

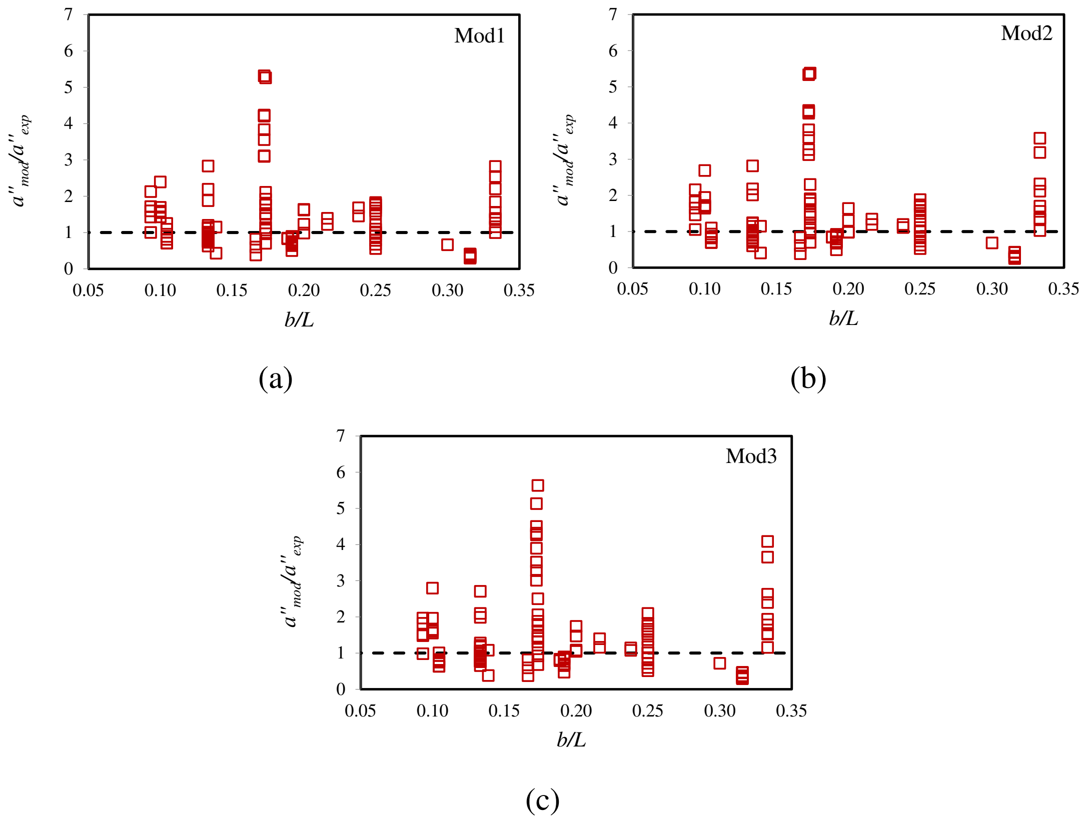

Figure 16. Performance of model for plastic rotation a''.

5. Fragility functions for PC and SFRC columns

After assessing the parametric sensitivity and quantifying the effects on the chord rotation of PC and SFRC columns under seismic load, this section aims to provide probabilistic assessments of failure or damage of PC and SFRC columns under lateral displacement caused by seismic loading and subsequently to inform the establishment of performance objectives, this section presents fragility analyses of flexure-dominated reinforced PC and SFRC concrete columns in different damage states.

The ASCE 41-17 standard provides a range of damage levels for concrete columns, which are used to assess the severity of the damage of the structures under seismic loading. The three main structural performance levels (while the two newly stipulated performance levels, namely Damage Control and Limited Safety in ASCE 41-17 are not considered herein) of RC columns during an earthquake specified in the current and all past versions of ASCE 41 are listed as follows:

1. Immediate Occupancy Performance Level (IO): At this state, no significant repair is required. Any minor cosmetic damage, such as surface cracking or spalling, can be repaired using low-strength concrete/slurry, epoxy injection, or other cosmetic repair methods.
2. Life Safety Performance Level (LS): A damaged column at this level may require repair or retrofitting to restore its strength and stiffness, and to prevent further damage. The appropriate repair techniques for LS level damage include those such as patching, overlaying, or jacketing of the column with fibre-reinforced polymer (FRP), steel. Additional reinforcement might also be required to add to the column to improve its strength and ductility.
3. Collapse Prevention Performance Level (CP): A severely damaged column requires significant repair or retrofitting to restore its capacity to carry loads and prevent collapse. The appropriate repair methods for CP level damage usually include jacketing the column with reinforced concrete or FRP, adding confinement to the existing reinforcement, or replacing the damaged portion of the column with a new reinforced concrete or steel section. The retrofitting design should consider the load path, displacement compatibility, and continuity of the structural system.

In the current work, adopting the method reported in [22], the fragility analyses of reinforced PC and SFRC columns are undertaken based on their lateral drift ratios aiming to evaluate the structural capacity of the columns under increasing levels of lateral displacement. Compared to methods such as incremental dynamic analysis (IDA) or incremental total hazard analysis (ITHA) for fragility analysis, where multiple dynamic analyses are demanded and they can be computationally intensive, one of the advantages of using lateral drift in fragility analysis is that it is a simple and easy-to-measure indicator of structural performance. Moreover, using lateral drift ratio in fragility analysis provides a clearer understanding of the level of deformation and damage that an individual element of the structure (referring to a RC column in the present work) is likely to undergo seismic loading. This information can be used to inform decisions about retrofitting and strengthening strategies, and can help to ensure that the structure is designed to withstand the seismic forces that it is likely to encounter in a given location. To generate the fragility curves for reinforced PC and RC columns, a threshold is established by defining three distinct damage states. The definitions of the three damage states are graphically depicted in Fig. 17, where:

1. Damage level 1 (*DL1*), which represents immediate occupancy performance level is defined as the lateral drift ratio corresponding to 80% of the yielding load on ascending part of the backbone curve; and
2. Damage level 2 (*DL2*), which represents life safety performance level is defined as the lateral drift ratio corresponding to 70% of the peak load on ascending part of the backbone curve; and
3. Damage level 3 (*DL3*), which represents collapse prevention performance level is defined as the lateral drift ratio corresponding to 25% drop in strength from the peak load on the descending branch of the backbone curve.
4. 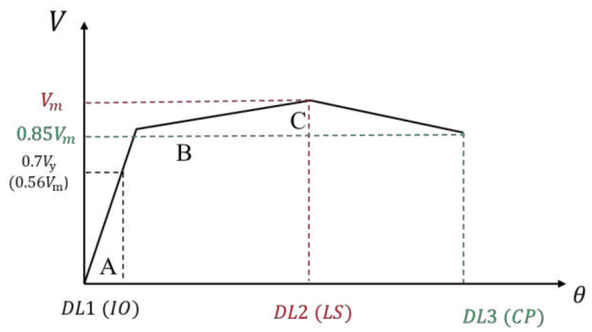

5. Figure 17. Definitions of alternative drift ratio for each damage state.
6.

Following the identification of the three damage states, the approach outlined in FEMA P-58 [12] were used to generate the fragility functions for PC and SFRC columns, where in order to characterize the damage states of the test series in the database, as commonly adopted in the literature [22, 24, 57], a cumulative distribution function based on the lognormal probability distribution Eq. (11) is assumed and applied.

$$P(DL > \theta_i) = \phi[\frac{1}{\beta_i}\ln\left(\frac{\theta}{\alpha_i}\right)] \quad (11)$$

where α_i and β_i are logarithmic standard deviation and mean value of the cumulative distribution function, respectively; ϕ is cumulative distribution function of the standard normal distribution; $P(DL > \theta_i)$ means that the probability of reaches or surpasses a specific level of damage ($DL1, DL2$ or $DL3$) that is determined by the attained drift ratio (θ_i). Specifically, α_i and β_i can be calculated as:

$$\beta_i = \sqrt{{\beta_r}^2 + {\beta_u}^2} \tag{12}$$

where $\beta_r = \sqrt{\frac{1}{1-M}\sum_{i=1}^{M}\left(\ln(\frac{\theta_i}{\alpha_i})\right)^2}$; M is the number of tests in each sub-data group; and based on the conditions given in FEMA P-58 [58] , $\beta_u = 0.1$ is used for the results in the current database.

$$\alpha_i = e^{\left(\frac{1}{M}\sum_{i=1}^{M}\ln(\theta_i)\right)} \tag{13}$$

As per the recommendations given in FEMA P-58, the established fragility functions should also pass the Lilliefors goodness-of-fit test to confirm the assumed lognormality for the data distribution. The criterion for the lognormality test is that the calculated indicator H (Eq. (14)) should not exceeds the critical value $H_{critical}$ at 5% significance level of each sub-data group (Eq. (16)).

$$H = max|P_i(\theta_i) - SM_i(\theta_i)| \tag{14}$$

where the sample cumulative distribution function$SM_i(\theta_i)$ is expressed as:

$$SM_i(\theta_i) = (i - 0.5)/M \tag{15}$$

the critical value $H_{critical}$ for each sub-data group is:

$$H_{critical} = 0.895/(M^{\frac{1}{2}} - 0.01 + 0.85M^{-\frac{1}{2}}) \tag{16}$$

In generating these fragility curves, 36 datasets of PC columns and 80 datasets of SFRC concrete columns were used at *DL1* and *DL2*; 36 datasets of PC columns and 80 datasets of SFRC concrete columns were used at *DL3*. The modelled fragility functions for both reinforced PC and SFRC concrete columns are plotted in Fig. 18 companying the related experimental results in the database. The calibrated α_i and β_i are reported in Table. 3 in conjunction with the Lilliefors goodness-of-fit test indicator H and the companion critical value $H_{critical}$. Since for all the cases $H < H_{critical}$, the validity of the developed frugality functions is proven. As shown in Fig. 18, the generated fragility functions align well with the results of the companion test campaigns. It is worth mentioning that in each damage state, compared to PC columns, a higher level of data dispersion is observed between the developed fragility model and the experimental data of SFRC columns, in particular at *DL2* and *DL3*. This can be attributed to the variations in the seismic performance of SFRC columns with varying fibres' parameters, particularly at the member level, fibre volume fraction. The developed fragility curves clearly show that the inclusion of fibres alters the failure probability of RC columns under seismic load.

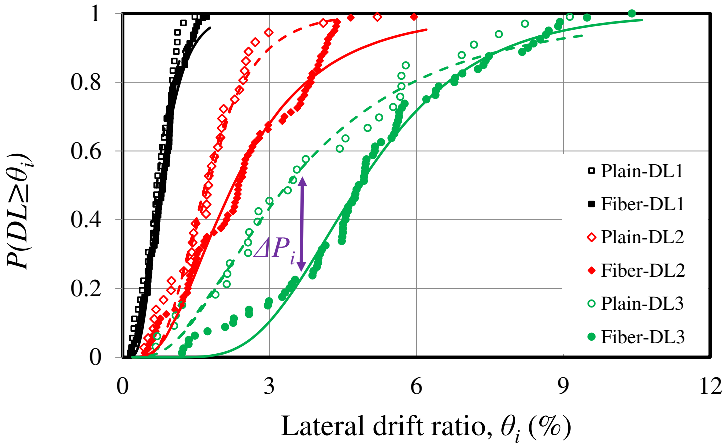

Figure 18. Fragility curves for the steel fibre reinforced- and plain- concrete columns.

Table 3. Parameters of lognormal distribution and the Kolmogorov-Smirnov goodness of-fit test results for plain and SFRC columns.

Concrete damage level	Parameters for lognormal distribution		Lilliefors goodness-of fit test results	
	α_i	β_i	H	$H_{crtical}$
DL1-Plain	0.70	0.47	0.09	0.28
DL2-Plain	1.69	0.45	0.10	0.30
DL3-Plain	3.36	0.68	0.07	0.26
DL1-SFRC	0.78	0.48	0.06	0.24
DL2-SFRC	2.26	0.60	0.07	0.26
DL3-SFRC	4.83	0.38	0.09	0.29

At *DL1*, PC and SFRC columns possess nearly the same failure probability up to that at the lateral drift ratio around 1%, while beyond this threshold, PC columns exhibit a higher failure probability compared to SFRC columns. Due to the small lateral rotation of both PC and SFRC columns at this level of damage, and the fact that the fibre's effect on preventing concrete cracks is not significant, the difference in the fragility functions between PC and SFRC columns is therefore considerably minor.

At *DL2*, a more pronounced difference can be seen between the fragility curves of PC and SFRC columns. PC columns exhibit a higher failure probability compared to SFRC columns for all ranges of lateral drift ratio in this damage state. The magnitude of the difference initially increases with increasing the lateral drift ratio to the lateral drift ratio of approximately 2.3 then converges. This indicates that the use of fibres can effectively control the cracking of concrete in a column and subsequently reduce its failure probability for the column deformed laterally at a moderate-to-high level. However, the influence of fibres becomes marginal when the lateral drift ratio is high, or when flexural cracks are larger.

At DL3, PC columns also exhibit a higher probability of failure compared to SFRC columns for a given lateral drift ratio, continuing the trend observed at DL2. However, there is a more rapid convergence between the two curves compared to what was seen previously. This can be explained by the fact that after forming large flexural cracks, fibres are either ruptured or completely pulled out from the concrete and hence lose their functions. Consequently, the failure probability of PC and SFRC columns becomes similar after the columns undergo a large lateral deformation.

Furthermore, the differences between the fragility curves of PC and SFRC columns in each damage state are quantified using an indicator ΔP_i [23] which is expressed as:

$$\Delta P_i = \left|P_{i-plain} - P_{i-SFRC}\right| \tag{17}$$

where $P_{i-plain}$ and P_{i-SFRC} are respectively the failure probability of PC and SFRC columns for a given lateral drift ratio at each damage level. Fig. 19 shows the relationships between ΔP_i and lateral drift ratio at all the three damage levels. It can be seen that at *DL1*, fibres have only marginal effects as the maximum value of ΔP_i is lower than 10%, while their influences are more evident at *DL2* and *DL3*. The maximum values of ΔP_i at *DL2* and *DL3* are 24% and 33%, restively, indicating that the presences of fibres in concrete columns can efficiently reduce the occurrence of failure of the columns deformed at a moderate-to-high level. The tails at the right-hand side of the curves for *DL2* and *DL3,* as that the curves tend to zero, confirm that PC and SFRC columns possess similar failure probability under seismic loading at a large lateral drift.

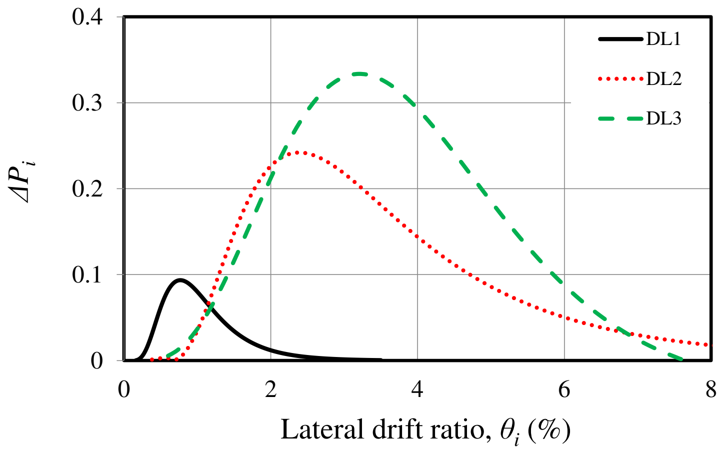

Figure 19. ΔP_f between steel fibre reinforced- and plain- concrete columns at each damage level.

6. CONCLUSION

This study presents thorough assessments of the seismic performance of steel fibre reinforced concrete (SFFRC) column, using a database of 116 individual tests of SFRC and plain concrete (PC) columns under cyclic lateral loading. Quantitative analysis of the database confirms that the slenderness of PC and SFRC columns is the primary factor affecting the lateral drift ratio of these columns under seismic load, with a higher drift ratio observed in slenderer RC columns. The effects of shear force ratio ($\frac{V}{bd\sqrt{f_c}}$), and volumetric ratio of transverse reinforcement ratio (ρ_{t_eq}) on the seismic behaviour of PC and SFRC columns are found to be nearly identical, in which a higher ρ_{t_eq} or a lower $\frac{V}{bd\sqrt{f_c}}$ leads to a higher lateral drift ratio of the columns at all the levels. Note that in this analysis fibres' effect is combined with the effect of volumetric ratio of transverse reinforcement through converting the fibres' inner confining effect to the equivalent external confinement provided by transverse reinforcements. However, the inclusion of fibres alters the effect of axial load ratio ($\frac{P}{A_g f_c}$) on the seismic behaviour of RC columns. For SFRC columns with a fibre volume fraction not higher than 0.75%, axial load ratio affects the rotation of columns in the same manner as PC columns, with the lateral drift ratio decreasing with increasing $\frac{P}{A_g f_c}$. While for SFRC columns with a relatively higher fibre dosage (> 0.75%), a higher lateral drift ratio at a moderate level of deformation is observed in some cases, due to the alignment of discrete fibres with the axial direction under higher axial loads. This phenomenon is particularly significant for columns deformed laterally at a moderate level, e.g., at the lateral drift corresponding to the peak shear force. The proposed models containing the identified factors, calibrated against the experimental database, can adequately predict the lateral drift ratio and plastic rotations at the yielding, peak, and ultimate points on the backbone curve for load-lateral rotation hysteresis loop PC and SFRC columns. Fragility analyses using the database indicate that the use of fibres in concrete columns can effectively control cracking and reduce the failure probability of the column when deformed laterally at a moderate-to-high level. However, the benefit of fibres becomes marginal at high lateral drift ratios or when flexural cracks are larger, as fibres lose their effectiveness and the failure probability of PC and SFRC columns becomes similar.

AUTHOR CONTRIBUTION STATEMENT

Daguang Han: Writing–original draft, Conceptualization. **Chunli Ying**: Writing – review & editing, Supervision. **Liyuan Chen**: Validation, Project administration. **Xuguang Wu**: Methodology, Investigation. **Huizhong Lin**: Methodology, Investigation.

DATA AVAILABILITY STATEMENT

The data are available from the corresponding author upon reasonable request.

REFERENCE

[1] Xie T, Mohamed Ali M, Elchalakani M, David M. Experimental and analytical study of ultrahigh-performance fiber-reinforced concrete curved beams. Journal of Structural Engineering. 2020;146:04019192.
[2] Xie T, Ali MM, Visintin P. Behaviour and analysis of ultra high performance fibre reinforced concrete (UHPFRC) skew slabs. Engineering Structures. 2019;199:109588.
[3] Mohebbi A. Development and seismic evaluation of pier systems w/pocket connections, CFRP tendons, and ECC/UHPC columns: University of Nevada, Reno; 2017.
[4] Ali MM, Mahdi S, Sheikh A, Elchalakani M, Xie T. Structural performance and analysis of

asymmetrically skewed and curved ultra-high performance fibre reinforced concrete slabs. Engineering Structures. 2022;252:113574.
[5] Mahdi S, Ali MM, Sheikh A, Elchalakani M, Xie T. An investigation into the feasibility of normal and fibre-reinforced ultra-high performance concrete multi-cell and composite sandwich panels. Journal of Building Engineering. 2021;41:102728.
[6] Zhang H, Zhang Y, Lu X, Duan Y, Zhang H. Influence of axial load ratio on the seismic behavior of steel fiber–reinforced concrete composite shear walls. Journal of structural engineering. 2020;146:04019171.
[7] Choun Y, Hahm D, Park J. Evaluation of Ultimate Pressure and Seismic Capacities of a Prestressed Concrete Containment Vessel Reinforced with Steel Fibers. 2013.
[8] Choun Y-S, Park J. Evaluation of seismic shear capacity of prestressed concrete containment vessels with fiber reinforcement. Nuclear Engineering and Technology. 2015;47:756-65.
[9] Schimmelpfennig K, Borgerhoff M. Development and application of a material law for steel-fibre-reinforced concrete with regard to its use for pre-stressed concrete reactor vessels. Nuclear engineering and design. 1995;156:181-8.
[10] ASCE. Seismic evaluation and retrofit of existing buildings. ASCE41-17. Reston, VA: ASCE: ASCE; 2017.
[11] American Concrete Institute. Building Code Requirements for Structural Concrete (ACI 318-19) and Commentary. ACI Committee 318, Farmington Hills, MI, USA; 2019.
[12] The American Society of Civil Engineers for the Federal Emergency Management Agency. Prestandard and Commentary for the Seismic Rehabilitation of Buildings, FEMA Publication no. 356. Washington, DC, USA; 2007.
[13] IBC. International Building Code. Washington, DC, USA: International Code Council; 2003.
[14] FIB. fib Model Code for Concrete Structures 2010. Lausanne: International Federation for Structural Concrete (FIB); 2013.
[15] European Committee for Standardization. Eurocode 8: Design of structures for earthquake resistance. Part 1 : General Rules, Seismic Actions and Rules for Buildings. Brussels: European Committee for Standardization; 2005. p. 1998-1.

[16] Di Domenico M, Ricci P, Verderame GM. Identifying and modeling ductile RC columns with deformed bars. Bulletin of Earthquake Engineering. 2023;21:2141-71.
[17] Inel M, Ozmen HB. Effects of plastic hinge properties in nonlinear analysis of reinforced concrete buildings. Engineering structures. 2006;28:1494-502.
[18] Sucuoğlu H, Günay MS. Generalized force vectors for multi-mode pushover analysis. Earthquake Engineering & Structural Dynamics. 2011;40:55-74.
[19] Xiao Y, Martirossyan A. Seismic performance of high-strength concrete columns. Journal of structural Engineering. 1998;124:241-51.
[20] Di Domenico M, Ricci P, Verderame GM. Empirical calibration of hysteretic parameters for modelling the seismic response of reinforced concrete columns with plain bars. Engineering Structures. 2021;237:112120.
[21] Mo Y-L, Wang S. Seismic behavior of RC columns with various tie configurations. Journal of Structural Engineering. 2000;126:1122-30.
[22] Goksu C. Fragility functions for reinforced concrete columns incorporating recycled aggregates. Engineering Structures. 2021;233:111908.
[23] Yu X-H, Dai K-Y, Li Y-S. Variability in corrosion damage models and its effect on seismic collapse fragility of aging reinforced concrete frames. Construction and Building Materials. 2021;295:123654.
[24] Gardoni P, Der Kiureghian A, Mosalam KM. Probabilistic capacity models and fragility estimates for reinforced concrete columns based on experimental observations. Journal of Engineering Mechanics. 2002;128:1024-38.

[25] Nagarajah R. Lateral load behavior of high-strength fiber-reinforced concrete columns: University of Nevada, Reno; 1997.
[26] Feng-lan L, Cheng-Kui H, Shi-Chen W, Jian-wei Q. Ductility of steel fiber reinforced high-strength concrete columns under cyclic loading. Engineering Mechanics. 2005;22:159-64.
[27] Sugano S, Kimura H, Shirai K. Study of new RC structures using ultra-high-strength fiber-reinforced concrete (UFC)-The challenge of applying 200 MPa UFC to earthquake resistant building structures. Journal of advanced concrete technology. 2007;5:133-47.
[28] Kawashima K, Zafra R, Sasaki T, Kajiwara K, Nakayama M. Effect of polypropylene fiber reinforced cement composite and steel fiber reinforced concrete for enhancing the seismic performance of bridge columns. Journal of Earthquake Engineering. 2011;15:1194-211.
[29] Caballero-Morrison KE, Bonet JL, Navarro-Gregori J, Martí-Vargas JR. Behaviour of steel-fibre-reinforced normal-strength concrete slender columns under cyclic loading. Engineering Structures. 2012;39:162-75.
[30] Caballero-Morrison KE, Bonet JL, Navarro-Gregori J, Serna-Ros P. An experimental study of steel fiber-reinforced high-strength concrete slender columns under cyclic loading. Engineering Structures. 2013;57:565-77.
[31] Ju Y, Wang D, Bai J. Seismic performance of reactive powder concrete columns. Journal of Harbin Institute of Technology. 2013;45:111-6.
[32] EL-Attar MM, El-Karmoty HZ, EL-Moneim AA. The behavior of ultra-high-strength reinforced concrete columns under axial and cyclic lateral loads. HBRC journal. 2016;12:284-95.
[33] Germano F, Tiberti G, Plizzari G, Colombo A. Experimental behavior of precast HSFRC columns in steel socket foundation under cyclic loads. Engineering Structures. 2015;102:230-48.
[34] Huang L, Xu L, Chi Y, Xu H. Experimental investigation on the seismic performance of steel–polypropylene hybrid fiber reinforced concrete columns. Construction and Building Materials. 2015;87:16-27.
[35] Liu KY, Liao WC, Yeh CC, Chang KC. Experimental study and prediction on the seismic performance of single bridge column with high strength, flowability, strain hardening steel fiber-reinforced concrete. Journal of the Chinese Institute of Civil and Hydraulic Engineering. 2015;27:287-300.
[36] Germano F, Tiberti G, Plizzari G. Experimental behavior of SFRC columns under uniaxial and biaxial cyclic loads. Composites Part B: Engineering. 2016;85:76-92.
[37] Zhang Y, Fan J, Fan W. Seismic fragility analysis of concrete bridge piers reinforced by steel fibers. Advances in Structural Engineering. 2016;19:837-48.
[38] Xu S, Wu C, Liu Z, Han K, Su Y, Zhao J, Li J. Experimental investigation of seismic behavior of ultra-high performance steel fiber reinforced concrete columns. Engineering Structures. 2017;152:129-48.
[39] Marchand P, Baby F, Khadour A, Rivillon P, Renaud J-C, Baron L et al. Response of UHPFRC columns submitted to combined axial and alternate flexural loads. Journal of Structural Engineering. 2019;145:04018225.
[40] He S, Deng Z, Yao J. Seismic behavior of ultra-high performance concrete long columns reinforced with high-strength steel. Journal of Building Engineering. 2020;32:101740.
[41] Aboukifa M, Moustafa MA. Experimental seismic behavior of ultra-high performance concrete columns with high strength steel reinforcement. Engineering Structures. 2021;232:111885.
[42] Chao S, Shamshiri M, Liu X, Palacios G, Schultz A, Nojavan A. Seismically robust ultra-high-performance fiber-reinforced concrete columns. ACI Structural Journal. 2021;118:17-32.
[43] HU R, FANG Z, XU B-d. Experimental Study on Seismic Behavior of UHPC Columns with Different Stirrup Ratios and Steel Fiber Contents. China Journal of Highway and Transport. 2021;34:65.
[44] Zhang J, Liu J, Li X, Cao W, Chen Z. Hysteretic behavior of steel fiber-reinforced high-strength concrete columns with high-strength steel bars. Structures: Elsevier; 2021. p. 1833-52.

[45] Zhang J, Li C, Feng G, Lu D. Seismic behavior of steel fiber high-strengthconcrete columns with HＲB600 steel bars. Journal of Building Structures2019. p. 113-21.

[46] Xie T, Ozbakkaloglu T. Behavior of steel fiber-reinforced high-strength concrete-filled FRP tube columns under axial compression. Engineering Structures. 2015;90:158-71.

[47] Li B, Harries KA. Seismic performance assessment of flexure-dominate FRP-confined RC columns using plastic rotation angle. Engineering Structures. 2018;172:453-71.
[48] Harries KA. ASCE 41 seismic assessment of FRP-repaired concrete columns. Journal of Composites for Construction. 2021;25:04021001.
[49] Barrera A, Bonet J, Romero ML, Miguel P. Experimental tests of slender reinforced concrete columns under combined axial load and lateral force. Engineering Structures. 2011;33:3676-89.
[50] Bae S, Bayrak O. Drift Capacity of Reinforced Concrete Columns. ACI structural journal. 2009;106.
[51] Ghannoum W, Saouma V, Haussmann G, Polkinghorne K, Eck M, Kang D-H. Experimental investigations of loading rate effects in reinforced concrete columns. Journal of Structural Engineering. 2012;138:1032-41.
[52] Xie T, Mohamed Ali M, Visintin P, Oehlers DJ, Sheikh A. Partial interaction model of flexural behavior of PVA fiber–reinforced concrete beams with GFRP bars. Journal of Composites for Construction. 2018;22:04018043.
[53] Sivaramakrishnan B. Non-linear modeling parameters for reinforced concrete columns subjected to seismic loads 2010.
[54] Paultre P, Eid R, Langlois Y, Lévesque Y. Behavior of steel fiber-reinforced high-strength concrete columns under uniaxial compression. Journal of Structural Engineering. 2010;136:1225-35.
[55] Chan Y-W, Chu S-H. Effect of silica fume on steel fiber bond characteristics in reactive powder concrete. Cement and concrete research. 2004;34:1167-72.
[56] Foster SJ. On behavior of high-strength concrete columns: cover spalling, steel fibers, and ductility. Structural Journal. 2001;98:583-9.
[57] Zhu L, Elwood K, Haukaas T. Classification and seismic safety evaluation of existing reinforced concrete columns. Journal of Structural Engineering. 2007;133:1316-30.
[58] Council AT, Program NEHR. Seismic performance assessment of buildings: Federal Emergency Management Agency; 2012.